Distributed Estimation of the Pelagic Scattering Layer using a Buoyancy Controlled Robotic System

Cong Wei[1][0000−0002−6552−7239] and Derek A. Paley[1,2][0000−0002−3086−2395]

[1] Institute for Systems Research, University of Maryland, College Park, MD 20742, USA
[2] Department of Aerospace Engineering, University of Maryland, College Park, MD 20742, USA
{weicong,dpaley}@umd.edu

Abstract. This paper formulates a strategy for Driftcam, an ocean-going robot system, to observe and track the motion of an ocean biological phenomenon called the pelagic scattering layer, which consists of organisms that migrate vertically in the water column once per day. Driftcam's horizontal motion is determined by the flow field and the vertical motion is regulated by onboard buoyancy control. In order to observe the evolution of the scattering layer, an ensemble Kalman filter is applied to estimate organism density; the density dynamics are propagated using the Perron-Frobenius operator. Multiple Driftcam are subject to depth regulation by open-loop and closed-loop controllers; a control strategy is proposed to track the peak of the density. Numerical simulations illustrate the efficacy of this strategy and motivate ongoing and future efforts to design a coordination formation algorithm for multi-agent Driftcam system to track the motion of the scattering layer, with implications for ocean monitoring.

Keywords: Density mapping · Ensemble Kalman filter · Scattering Layer

1 Introduction

This paper addresses the problem of underwater mapping of a marine biological system called the pelagic scattering layer. An ocean-going system called Driftcam is deployed to perform the mapping, ideally in a group. This robotic system is propelled by ocean currents and is used for counting and measuring organisms in the pelagic scattering layer with a high-definition low-light camera [22]. Depth is regulated through a piston pump engine, which pumps oil into an external bladder that can change buoyancy by its expandable volume [1].

The pelagic scattering layer, also referred to as the sound scattering layer, is a biological layer in the ocean consisting of a variety of marine animals[3]. An important feature of the pelagic scattering layer is the daily movement of organisms from the deep ocean during the day to a shallow depth during the night [20]. This diel vertical migration represents the largest biology movement on the planet in terms of biomass, number of individuals, and species[4] and plays a key role in structuring ecological and physic-

[3] https://en.wikipedia.org/wiki/Deep_scattering_layer
[4] https://oceanexplorer.noaa.gov/technology/development-partnerships/21scattering-layer/features/scattering-layer/scattering-layer.html

ochemical processes, as well as the biological carbon pump of vast oceanic ecosystems [3].

Despite the importance of the scattering layer, we lack knowledge of its biological features and biogeochemical processes [10], because the scattering layer is difficult to sample and observe in real time. Most sampling and sensing systems either cause disturbances or collect indirect data, resulting in inaccuracy [2, 16]. The untethered Driftcam system modeled in this paper provides a direct observation of the organisms living in the scattering layer [1]. This sampling problem is an example of a dynamic, data-driven application system in which the collection of measurements is used to update a model, which in turn is used to guide the collection of subsequent measurements.

Our work seeks a solution for long-endurance and large-scale sampling over mesopelagic[5] ocean space. The design and development of a long-endurance passive marine sensor system makes it possible to sample large-scale ocean environments for specified phenomena of interest [11, 12, 21]. Purely passive drifters like the Argo system are not able to automatically achieve the configurations that improves sampling efficiency [19]. Actuated vehicles like autonomous surface vehicles and autonomous underwater vehicles are used to achieve faster surveys in the dynamic marine environment [9], but they may rely on prior knowledge of the flow field and require a large number of vehicles, depending on the scale of the region of interest. Multi-agent autonomous drifters are also deployed in a depth-holding configuration to measure the internal waves near the shore [12], however, this configuration is more suitable to monitoring ocean dynamics or biological systems occurring at relative limited depth interval. Another ocean sampling method includes using actuated autonomous underwater vehicles to track a patch of interest tagged by Lagrangian drifters. [4]. An adaptive sampling strategy [5] uses feedback control to redesign paths in response to updated sensor measurements, such as for sampling ocean features [15, 18].

This paper aims at identifying the depth and vertical distribution of the scattering layer by sampling the density of organisms using onboard cameras, which use image processing to measure organism density locally. The vertical depth dynamics of the scattering layer determines the density propagation over time. An estimator is used to recover the density field from discrete density measurements by one or more Driftcam. The goal is to collect data that minimizes the estimation error of scattering layer density, e.g., by tracking the density peak with a Driftcam using closed-loop control.

The contributions of this paper are (1) a dynamic model of organism density in the scattering layer using the Perron-Frobenius operator; (2) an estimation framework that assimilates discrete measurements taken by one or more Driftcam to reconstruct the density and identify its peak using an ensemble Kalman filter; (3) and an adaptive sampling strategy based on the recovered density map in which one or more Driftcam tracks the peak density using closed-loop control.

The paper is organized as follows. Section 2 gives a brief description of the Perron-Frobenius operator and the ensemble Kalman filter. Section 3 models the density propagation based on the dynamics of diel vertical migration. The ensemble Kalman filter is applied to recover the density field from measurements collected by one or more Drift-

[5] https://ocean.si.edu/ecosystems/deep-sea/deep-sea

cam. Numerical simulations in Section 4 illustrate the performance of the sampling method. Section 5 summarizes the paper and ongoing and future work.

2 Preliminary

2.1 Perron-Frobenius Operator

The Perron-Frobenius (PF) operator is used in ergodic theory to study measure-theoretic characterization. This is a brief introduction; detailed information can be found in [6, 8]. Let $\mathbb{X}$ be a compact manifold and $f : \mathbb{X} \to \mathbb{X}$ be a smooth time invariant vector field. Consider the following time invariant system

$$\dot{x} = f(x). \tag{1}$$

Let $\phi_f : \mathbb{R} \times \mathbb{X} \to \mathbb{X}$ be the solution of system (1), i.e., $x = \phi_f(t, x_0)$ satisfies (1) with initial condition $x(0) = x_0$.

Definition 1. *A semigroup of operator $\mathcal{P}^\tau : \tau > 0$ is said to be the PF operator if $\mathcal{P}^\tau : L^1(\mathbb{X}) \to L^1(\mathbb{X})$ is defined by [6]*

$$\mathcal{P}^\tau \rho(\cdot) = \rho \circ \phi_f(-\tau, \cdot)|\det(D_x \phi_f(-\tau, \cdot))|, \tag{2}$$

where D_x represents the Jacobian matrix with respect to state variable x.

If $\rho(\cdot)$ is a probability density (PDF) with respect to an absolutely continuous probability measure v, then $\mathcal{P}^\tau \rho$ is another PDF with respect to the absolutely continuous probability measure $v \circ \phi(-\tau, \cdot)$. Specifically,

$$\int_B \mathcal{P}^\tau \mathrm{d}v = \int_{\phi_f(-\tau, B)} \rho \mathrm{d}v, \tag{3}$$

for any v-measurable set B [14]. The PF operator transport a density function with time according to the flow of the system dynamics.

2.2 Ensemble Kalman filter

The ensemble Kalman filter (EnKF) is an Monte Carlo approximation of the Kalman filter that stores, propagates and updates an ensemble of vectors to approximate the state distribution [13, 17]. Consider a nonlinear dynamic system and a linear measurement equation,

$$x(t_{k+1}) = f(x_k) + w(t_{k+1}) \tag{4a}$$

$$y(t_{k+1}) = Hx(t_{k+1}) + v(t_{k+1}), \tag{4b}$$

where $x(t_k), w(t_k) \in \mathbb{R}^n$ and $y(t_k), v(t_k) \in \mathbb{R}^m$. Assume that $w(t_k)$ and $v(t_k)$ are zero-mean white noise with covariance matrices $Q(t_k)$ and $R(t_k)$, respectively. Moreover, $x(t_0), w(t_k)$ and $v(t_k)$ are uncorrelated. For ensemble Kalman filter, the distribution is replaced by a collection of realizations called an ensemble. Let

$$X = [x_1, \cdots, x_N] = [x_i] \tag{5}$$

be an $n \times N$ matrix, where x_i is a sample from prior distribution. Matrix X is the prior ensemble. In the same way, the distribution of measurement is represented by

$$Y = [y_1, \cdots, y_N] = [y_i]. \tag{6}$$

Here we show only the result of ensemble Kalman filter; detailed information can be found in [7, 13, 17]. The forecast of EnKF is

$$\tilde{X}(t_{k+1}) = f(\hat{X}(t_k)) + W(k) \tag{7a}$$

$$E(\tilde{X}(t_{k+1})) = \frac{1}{N}\sum_{i=1}^{N} x_i, \;\; C = \frac{AA^T}{N-1}, \tag{7b}$$

where

$$A = \tilde{X}(t_{k+1}) - E(\tilde{X}(t_{k+1})). \tag{8}$$

The update is given by

$$\hat{X}(t_{k+1}) = \tilde{X}(t_{k+1}) + CH^T(HCH^T + R)^{-1}(Y - HX). \tag{9}$$

The EnKF implemented below has as state vector the density of the scattering layer over a range of discrete depths; it uses the PF operator to propagate those density estimates forward in time.

3 Estimation of the scattering layer

The depth ζ of the scattering layer at time t is modeled dynamically as follows:

$$\dot{\zeta} = -\omega(\zeta(0) - \zeta_0)\sin(\omega t) \tag{10a}$$

$$\dot{t} = 1 \tag{10b}$$

where ω indicates the frequency of vertical migration (one cycle per 24 hours). To mimic the width contraction at the surface, assume $\zeta_0 = \alpha\zeta(0),\ \alpha \in (0.5, 1)$. The dynamics (10) translate the organism density vertically. Define $\phi(t, \zeta(0)) : \mathbb{R} \times \mathbb{R}^+ \to \mathbb{R}$, as the flow map, where

$$\phi(t, \zeta(0)) = \zeta(0)[\alpha + (1-\alpha)\cos\omega t]. \tag{11}$$

The density at a depth $\zeta_d \in \mathbb{R}^-$ can be predicted by the PF operator, i.e.,

$$\rho(t_k, \zeta_d) = \rho(0, \phi(-t_k, \zeta_d))D(t_k, 0) \tag{12a}$$

$$\rho(t_{k+1}, \zeta_d) = \rho(0, \phi(-t_{k+1}, \zeta_d))D(t_{k+1}, 0), \tag{12b}$$

where $D(t_k, 0) = 1/[\alpha + (1-\alpha)\cos\omega t_k]$

$$D(t_{k+1}, t_k) \triangleq \frac{\alpha + (1-\alpha)\cos\omega t_k}{\alpha + (1-\alpha)\cos\omega t_{k+1}}. \tag{13}$$

The density propagation at ζ from t_k to t_{k+1} derived from (12) is

$$\rho(t_{k+1}, \zeta(t_{k+1})) = \Delta(t_{k+1}, t_k)\rho(t_k, \zeta(t_k)). \tag{14}$$

where

$$\Delta(t_{k+1}, t_k) = D(t_{k+1}, t_k)\frac{\rho(0, \phi(-t_{k+1}, \zeta_d))}{\rho(0, \phi(-t_k, \zeta_d))}. \tag{15}$$

Consider M Driftcam at depths $[z_{D_1}, \cdots, z_{D_M}]^T$; each collects a noisy measurement at a constant time step $\tau_m > t_{k+1} - t_k$; the measurement is $y(t_k) \in \mathbb{R}^M$. Discretizing the full ocean depth into n_o levels, let $\mathbb{R}^{n_o} \ni x(t_k) \triangleq [\rho(t_k, \zeta_i(t_k))]$. Based on density propagation model (14), the density state-space model is

$$x(t_{k+1}) = \Delta(t_{k+1}, t_k)x(t_k) + w(t_{k+1}), \qquad w(t_{k+1}) \sim \mathcal{N}(0, Q(t_{k+1})) \tag{16a}$$

$$t_{k+1} = t_k + \tau_p \tag{16b}$$

$$y(t_{k+1}) = H(t_{k+1})x(t_{k+1}) + v(t_{k+1}), \qquad v(t_{k+1}) \sim \mathcal{N}(0, R(t_{k+1})), \tag{16c}$$

where

$$H_{lj}(t_k) = \begin{cases} 1 & \text{if } z_{D_l}(t_k) = \zeta_j(t_k) \\ 0 & \text{otherwise.} \end{cases}$$

We design an unbiased estimator following the steps from (5)–(9). The result is

$$\hat{\mathbf{X}}(k) = [\hat{x}_1(k), \hat{x}_2(k), \cdots, \hat{x}_N(k)] \in \mathbb{R}^{n_o \times N}.$$

The EnKF forecast step obtains

$$\tilde{x}_i(t_{k+1}) = \Delta(t_{k+1}, t_k)\hat{x}_i(t_k) + w_i(t_{k+1}),\ w_i(t_{k+1}) \sim \mathcal{N}(0, Q(t_{k+1})).$$

Forecast covariance is calculated from (7b). The observation $y(k+1)$ here forms a matrix, $\tilde{\mathbf{Y}} \in \mathbb{R}^{M \times N}$, given by

$$\tilde{\mathbf{Y}}(t_{k+1}) = [\tilde{y}_1(t_{k+1}), \cdots, \tilde{y}_N(t_{k+1})],$$

where $\tilde{y}_i(t_{k+1}) = y_i(t_{k+1}) + v(t_{k+1})$. The updated ensemble $\hat{\mathbf{X}}$ is calculated as follows [13],

$$\hat{\mathbf{X}}(t_{k+1}) = \tilde{\mathbf{X}}(t_{k+1}) + K[\tilde{\mathbf{Y}}(t_{k+1}) - H(t_k)\tilde{\mathbf{X}}(t_{k+1})],$$

where

$$K = CH^T(t_{k+1})[H(t_{k+1})CH^T(t_{k+1}) + R(t_{k+1})]^{-1}.$$

The following section illustrates the scattering layer modeling and estimation framework.

4 Numerical Results

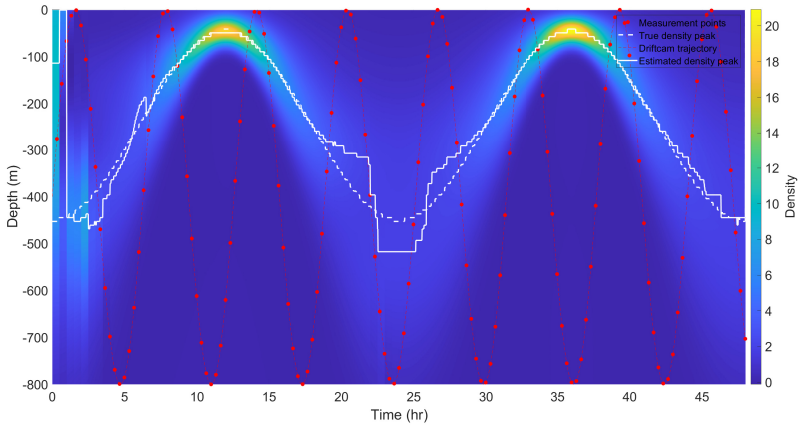

(a) Density over time estimated by a single Driftcam.

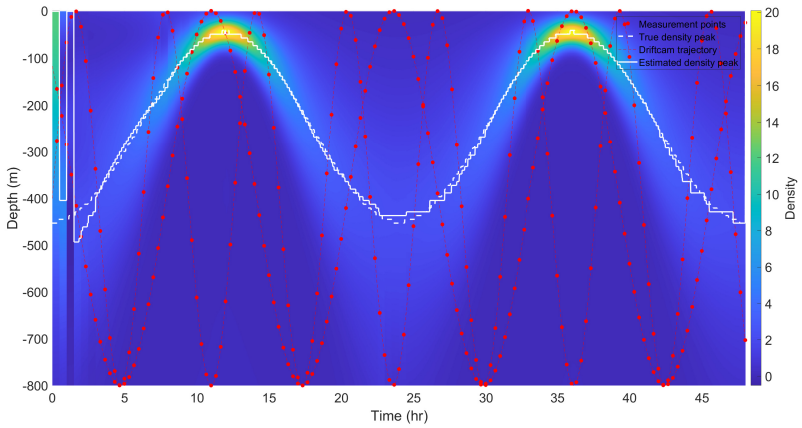

(b) Density over time estimated by two Driftcam.

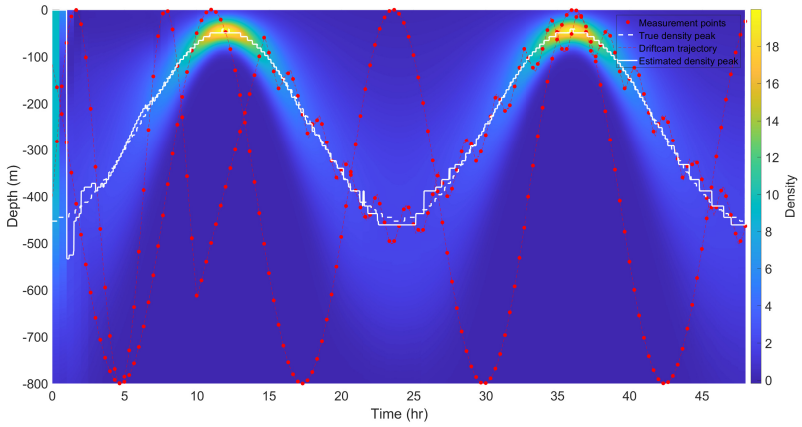

(c) Density over time estimated by two Driftcam; one is equipped with a closed-loop controller that tracks the peak of the estimate, when the ensemble covariance is sufficiently low.

Fig. 1. Estimation of scattering layer density over time, with one or two Driftcam

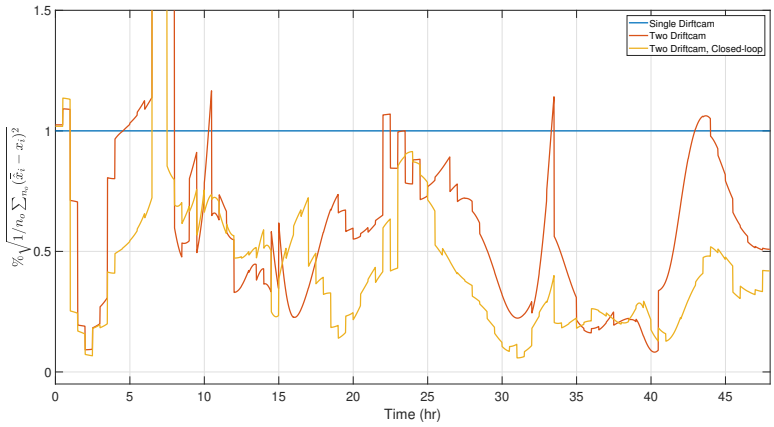

(a) Root-mean-square error

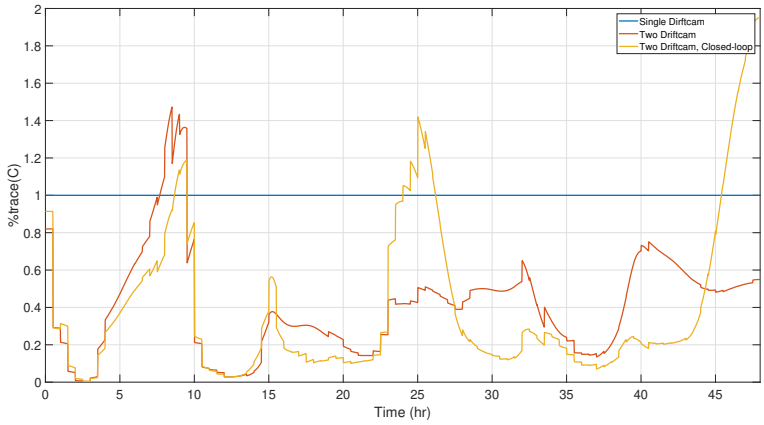

e

(b) Trace of ensemble covariance

Fig. 2. Performance evaluation for open- and closed-loop Driftcam control. All the data is normalized by that from the single Driftcam case.

This section presents three cases of scattering layer sampling: a single Driftcam, two Driftcam, and two Driftcam with a closed-loop tracking controller. All the cases share the same period of diel migration (24 hours), the same number of ensemble members $N = 100$, and depth resolution $n_o = 100$.

In the first case, one Driftcam is commanded to perform sinusoidal motion from -800m to 0m with frequency 0.15/hour. The Driftcam collects a density measurement every 30min, shown as red dots on Fig 1(a). The average vertical speed is 7 cm/s. Fig 1(a) shows that a single Dirftcam is able to map the density field and identify the

density peak as indicated by the white line in Fig 1(a). However, performance improves with a second Driftcam as shown next.

The second sampling result is for the case with two Driftcam. The second Driftcam is commanded to perform sinusoidal motion from -800m to 0m. From Fig 1(b), the quality of mapping is improved compared to a single Driftcam, especially when the organisms are sparsely distributed at the bottom. In the last case, after being deployed for a certain time (10 hours), a feedback controller is activated when the trace of ensemble covariance is below a threshold (20). This controller drives one Driftcam to track the estimated density peak. Fig 2(a) and Fig 2(b) suggest that more Driftcam deployed in the region of interest can reduce estimation error and its covariance. The estimation error is the smallest in the closed-loop control case; however, the trace of the ensemble covariance becomes higher.

5 Conclusion

This work presents an ocean-sampling strategy for a buoyancy-driven underwater vehicle designed to observe the density field of the pelagic scattering layer. The strategy is designed based on modeling the density dynamics by the Perron-Frobenius operator. Samples of the density field are assimilated by an ensemble Kalman filter. This paper reveals two strategies to improve the estimation performance either by deploying more Driftcam or by closed-loop control. In ongoing work, the strategy will be extended to multiple Driftcam for higher spatial dimensions. Additionally, a coordinated controller may be incorporated into the sampling strategy to regulate the Driftcam motion relative to one another.

References

1. Berkenpas, E.J., Henning, B.S., Shepard, C.M., Turchik, A.J., Robinson, C.J., Portner, E.J., Li, D.H., Daniel, P.C., Gilly, W.F.: A buoyancy-controlled Lagrangian camera platform for *in situ* imaging of marine organisms in midwater scattering layers. IEEE Journal of Oceanic Engineering **43**(3), 595–607 (2018). https://doi.org/10.1109/JOE.2017.2736138
2. Blanluet, A., Doray, M., Berger, L., Romagnan, J.B., Le Bouffant, N., Lehuta, S., Petitgas, P.: Characterization of sound scattering layers in the Bay of Biscay using broadband acoustics, nets and video. PLOS ONE **14**(10), 1–19 (2019). https://doi.org/10.1371/journal.pone.0223618
3. Brodeur, R., Pakhomov, E.: Nekton. In: Cochran, J.K., Bokuniewicz, H.J., Yager, P.L. (eds.) Encyclopedia of Ocean Sciences (Third Edition), pp. 582–587. Academic Press, Oxford, third edn. (2019)
4. Das, J., Py, F., Maughan, T., O'Reilly, T., Messié, M., Ryan, J., Sukhatme, G.S., Rajan, K.: Coordinated sampling of dynamic oceanographic features with underwater vehicles and drifters. The International Journal of Robotics Research **31**(5), 626–646 (2012). https://doi.org/10.1177/0278364912440736
5. Fiorelli, E., Leonard, N.E., Bhatta, P., Paley, D.A., Bachmayer, R., Fratantoni, D.M.: Multi-auv control and adaptive sampling in Monterey Bay. IEEE Journal of Oceanic Engineering **31**, 935–948 (10 2006). https://doi.org/10.1109/JOE.2006.880429

6. Froyland, G., Padberg, K.: Almost-invariant sets and invariant manifolds-connecting probabilistic and geometric descriptions of coherent structures in flows. Physica D: Nonlinear Phenomena **238**(16), 1507–1523 (2009). https://doi.org/https://doi.org/10.1016/j.physd.2009.03.002
7. Gillijns, S., Mendoza, O., Chandrasekar, J., De Moor, B., Bernstein, D., Ridley, A.: What is the ensemble Kalman filter and how well does it work? In: Proceedings of the IEEE American Control Conference. pp. 4448–4453 (2006). https://doi.org/10.1109/ACC.2006.1657419
8. Goswami, D., Thackray, E., Paley, D.A.: Constrained Ulam dynamic mode decomposition: Approximation of the Perron-Frobenius operator for deterministic and stochastic systems. IEEE Control Systems Letters **2**(4), 809–814 (2018). https://doi.org/10.1109/LCSYS.2018.2849552
9. Hansen, J., Manjanna, S., Li, A.Q., Rekleitis, I., Dudek, G.: Autonomous marine sampling enhanced by strategically deployed drifters in marine flow fields. In: Proceedings of the OCEANS MTS/IEEE Charleston. pp. 1–7 (2018). https://doi.org/10.1109/OCEANS.2018.8604873
10. Haëntjens, N., Della Penna, A., Briggs, N., Karp-Boss, L., Gaube, P., Claustre, H., Boss, E.: Detecting mesopelagic organisms using biogeochemical-argo floats. Geophysical Research Letters **47**(6), e2019GL086088 (2020). https://doi.org/https://doi.org/10.1029/2019GL086088
11. Hsieh, M.A., Hajieghrary, H., Kularatne, D., Heckman, C.R., Forgoston, E., Schwartz, I.B., Yecko, P.A.: Small and adrift with self-control : Using the environment to improve autonomy. Proceedings of the International Symposium on Robotics Research pp. 1–16 (2015). https://doi.org/10.1007/978-3-319-60916-4_22
12. Jaffe, J.S., Franks, P.J., Roberts, P.L., Mirza, D., Schurgers, C., Kastner, R., Boch, A.: A swarm of autonomous miniature underwater robot drifters for exploring submesoscale ocean dynamics. Nature Communications **8**, 1–8 (2017). https://doi.org/10.1038/ncomms14189
13. Katzfuss, M., Stroud, J.R., Wikle, C.K.: Understanding the ensemble kalman filter. The American Statistician **70**(4), 350–357 (2016). https://doi.org/10.1080/00031305.2016.1141709
14. Klus, S., Nüske, F., Koltai, P., Wu, H., Kevrekidis, I., Schütte, C., Noé, F.: Data-driven model reduction and transfer operator approximation. Journal of Nonlinear Science **28**(4), 985–1010 (2018)
15. Kularatne, D., Hsieh, A.: Tracking attracting lagrangian coherent structures in flows. In: Proceedings of Robotics: Science and Systems. Rome, Italy (July 2015). https://doi.org/10.15607/RSS.2015.XI.021
16. Lavery, A.C., Chu, D., Moum, J.N.: Measurements of acoustic scattering from zooplankton and oceanic microstructure using a broadband echosounder. ICES Journal of Marine Science **67**(2), 379–394 (10 2009). https://doi.org/10.1093/icesjms/fsp242
17. Mandel, J.: A brief tutorial on the Ensemble Kalman Filter (2009). https://doi.org/10.48550/ARXIV.0901.3725, https://arxiv.org/abs/0901.3725
18. Michini, M., Hsieh, M.A., Forgoston, E., Schwartz, I.B.: Robotic tracking of coherent structures in flows. IEEE Transactions on Robotics **30**(3), 593–603 (2014). https://doi.org/10.1109/TRO.2013.2295655
19. Roemmich, D., Alford, M.H., Claustre, H., Johnson, K., King, B., Moum, J., Oke, P., Owens, W.B., Pouliquen, S., Purkey, S., Scanderbeg, M., Suga, T., Wijffels, S., Zilberman, N., Bakker, D., Baringer, M., Belbeoch, M., Bittig, H.C., Boss, E., Calil, P., Carse, F., Carval, T., Chai, F., Conchubhair, D.Ó., d'Ortenzio, F., Dall'Olmo, G., Desbruyeres, D., Fennel, K., Fer, I., Ferrari, R., Forget, G., Freeland, H., Fujiki, T., Gehlen, M., Greenan, B., Hallberg, R., Hibiya, T., Hosoda, S., Jayne, S., Jochum, M., Johnson, G.C., Kang, K., Kolodziejczyk, N., Körtzinger, A., Traon, P.Y.L., Lenn, Y.D., Maze, G., Mork, K.A., Morris, T., Nagai, T.,

Nash, J., Garabato, A.N., Olsen, A., Pattabhi, R.R., Prakash, S., Riser, S., Schmechtig, C., Schmid, C., Shroyer, E., Sterl, A., Sutton, P., Talley, L., Tanhua, T., Thierry, V., Thomalla, S., Toole, J., Troisi, A., Trull, T.W., Turton, J., Velez-Belchi, P.J., Walczowski, W., Wang, H., Wanninkhof, R., Waterhouse, A.F., Waterman, S., Watson, A., Wilson, C., Wong, A.P.S., Xu, J., Yasuda, I.: On the future of argo: A global, full-depth, multi-disciplinary array. Frontiers in Marine Science **6** (2019). https://doi.org/10.3389/fmars.2019.00439

20. Seki, M.P., Polovina, J.J.: Ocean gyre ecosystems. In: Cochran, J.K., Bokuniewicz, H.J., Yager, P.L. (eds.) Encyclopedia of Ocean Sciences (Third Edition), pp. 753–758. Academic Press, Oxford, third edition edn. (2019)
21. Subbaraya, S., Breitenmoser, A., Molchanov, A., Müller, J., Oberg, C., Caron, D.A., Sukhatme, G.S.: Circling the seas: Design of Lagrangian drifters for ocean monitoring. IEEE Robotics & Automation Magazine **23**, 42–53 (2016)
22. Suitor, R., Berkenpas, E., Shepard, C.M., Abernathy, K., Paley, D.A.: Dynamics and control of a buoyancy-driven underwater vehicle for estimating and tracking the scattering layer. In: Proceedings of the IEEE American Control Conference (2022)